Inorganic Chemistry

Article

pubs.acs.org/IC

New Insights into the Electronic Structure and Reactivity of One-Electron Oxidized Copper(II)-(Disalicylidene)diamine Complexes

Kazutaka Asami,[†] Kazuaki Tsukidate,[†] Satoshi Iwatsuki,[‡] Fumito Tani,[§] Satoru Karasawa,[∥] Linus Chiang,[⊥] Tim Storr,[⊥] Fabrice Thomas,[⊗] and Yuichi Shimazaki*[,†]

[†]College of Science, Ibaraki University, Bunkyo, Mito 310-8512, Japan

[‡]Department of Chemistry, Konan University, Higashinada-ku, Kobe 658-8501, Japan

[§]Institute for Materials Chemistry and Engineering, Kyushu University, Higashi-ku, Fukuoka 812-8581, Japan

[∥]Graduate School of Pharmaceutical Sciences, Kyushu University, Higashi-ku, Fukuoka 812-8582, Japan

[⊥]Department of Chemistry, Simon Fraser University, Burnaby, British Columbia, Canada

[⊗]Département de Chimie Moléculaire-Chimie Inorganique Redox Biomimétique (CIRE) - UMR CNRS 5250, Université Joseph Fourier, B. P. 53, 38041 Grenoble cedex 9, France

Supporting Information

ABSTRACT: The neutral and one-electron oxidized Cu(II) six-membered chelate **1,3-Salcn** (**1,3-Salcn** = *N,N′*-bis(3,5-di-*tert*-butylsalicylidene)-1,3-cyclohexanediamine) complexes have been investigated and compared with the five-membered chelate **1,2-Salcn** (*N,N′*-bis(3,5-di-*tert*-butylsalicylidene)-1,2-cyclohexane-(1*R*,2*R*)-diamine) complexes. Cyclic voltammetry of Cu(**1,3-Salcn**) showed two reversible redox waves at 0.48 and 0.68 V, which are only 0.03 V higher than those of Cu(**1,2-Salcn**). Reaction of Cu(**1,3-Salcn**) with 1 equiv of $AgSbF_6$ afforded the oxidized complex which exists as a ligand-based radical species in solution and in the solid state. The X-ray crystal structure of the oxidized complex, [Cu(**1,3-Salcn**)]**SbF**$_6$, exhibited an asymmetric metal binding environment with a longer Cu−O bond and quinoid distortion in the phenolate moiety on one side, demonstrating at least partial ligand radical localization in the solid state. The ligand oxidation is also supported by XPS and temperature dependent magnetic susceptibility. The electronic structure of the [Cu(**1,3-Salcn**)]$^+$ complex was further probed by UV−vis−NIR, resonance Raman, and electron paramagnetic resonance (EPR) measurements, and by theoretical calculations, indicating that the phenoxyl radical electron is relatively localized on one phenolate moiety in the molecule. The reactivity of [Cu(**1,3-Salcn**)]$^+$ with benzyl alcohol was also studied. Quantitative conversion of benzyl alcohol to benzaldehyde was observed, with a faster reaction rate in comparison with [Cu(**1,2-Salcn**)]$^+$. The kinetic isotope effect (KIE = k(H)/k(D)) of benzyl alcohol oxidation by [Cu(**1,3-Salcn**)]$^+$ was estimated to be 13, which is smaller than the value reported for [Cu(**1,2-Salcn**)]$^+$. The activation energy difference between [Cu(**1,2-Salcn**)]$^+$ and [Cu(**1,3-Salcn**)]$^+$ was in good agreement with the energy calculated from KIE. This correlation suggests that the Cu(II)-phenoxyl radical species, characterized for [Cu(**1,2-salcn**)]$^+$ is more reactive for hydrogen abstraction from benzyl alcohol in comparison to the 1:1 mixture of Cu(III)-phenolate and Cu(II)-phenoxyl radical species, [Cu(**1,2-Salcn**)]$^+$. Thus, the Cu(II)-phenoxyl radical species accelerates benzyl alcohol oxidation in comparison with the Cu(III)-phenolate ground state complex, in spite of the similar activated intermediate and oxidation pathway.

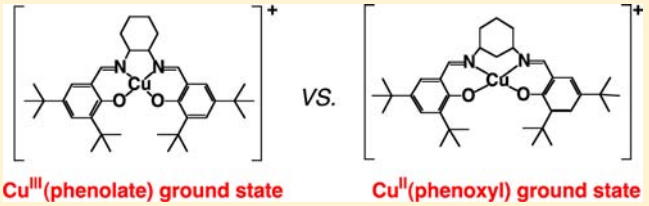

INTRODUCTION

Interest in metal-catalyzed reactions in chemical and biological systems has prompted studies of the redox chemistry of metal complexes, which has afforded significant insights into the reaction mechanisms of many useful homogeneous catalytic reactions and reactions of metalloenzymes.[1] In the course of these studies, a large number of novel complexes have been prepared,[2−5] and it has been increasingly recognized that radical species formed as a result of redox reactions are especially important in biological systems. Thus, radicals of amino acid residues, such as tyrosyl, cysteinyl, glycyl, and tryptophyl radicals, are now known to form in the course of certain enzymatic reactions.[6,7]

Phenoxyl radical formation from tyrosyl residues has been well established in metalloenzymes such as class I ribonucleotide reductase and prostaglandin endoperoxide synthase.[6,7] It was discovered that the phenoxyl radical can bind to a metal ion as an open-shell ligand fulfilling the role of an organic radical cofactor in the metalloenzyme, galactose oxidase (GO), which is a single copper oxidase catalyzing the two-electron oxidation of a primary alcohol to the aldehyde (Figure 1).[8] A copper(III) species had once been considered to be a possibility as the active form of GO,[9] but many physicochemical studies revealed the formation of a Cu(II)−phenoxyl radical species.[8,10,11] A

Received: August 24, 2012
Published: October 31, 2012

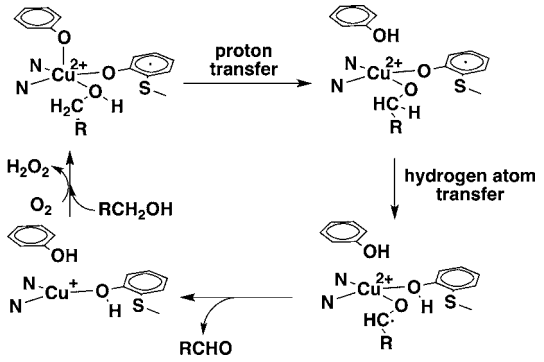

Figure 1. Proposed catalytic alcohol oxidation mechanism of GO.

proposed mechanism which has been generally accepted indicates that the oxidized form of GO in the Cu(II)-tyrosine radical state binds the primary alcohol in the fourth equatorial position and that subsequent hydrogen atom abstraction and electron transfer lead to formation of the aldehyde via the ketyl radical intermediate and the reduced form of GO.[8] For an improved understanding of the detailed mechanism of GO and the properties of the metal complexes with the coordinated phenoxyl radical, many metal−phenolate complexes have been synthesized and characterized.[12,13]

Depending on the relative energies of the redox-active orbitals, a metal complex with a noninnocent ligand exists in two limiting descriptions, either a metal−ligand radical ($M^{n+}(L^{\bullet})$) or a high valent metal ($M^{(n+1)+}(L^{-})$) complex.[14,15] Oxidized metal salen-type complexes are known to exist in either form, and the factors that control the locus of oxidation in these complexes are being actively pursued. The one-electron oxidized Ni(**1,2-Salcn**) complex (Figure 2) exists in the ligand

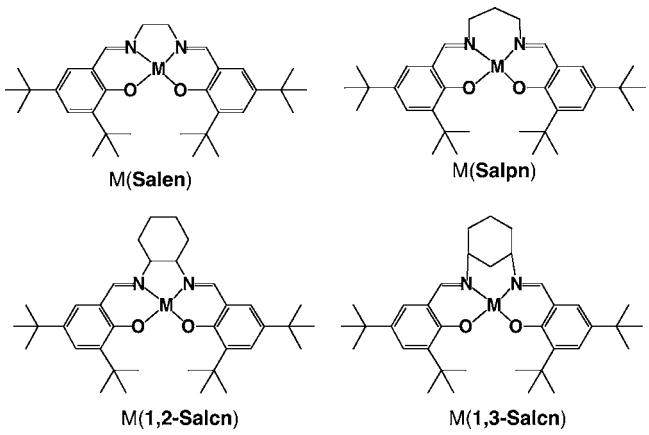

Figure 2. Structures of some salen-type complexes: M(**Salen**), M(**Salpn**), M(**1,2-Salcn**), and M(**1,3-Salcn**).

radical form in the solid state and in solution, and yet the presence of coordinating ligands and/or solvent shifts the locus of oxidation to the nickel center, forming a Ni(III) complex.[16−20] This result demonstrates that a subtle change of electronic structure can have a significant effect on the locus of oxidation in these systems. Building on these results, we have reported on the electronic structure of one-electron oxidized group 10 metal **Salpn** complexes with a 6-membered chelate backbone.[20] The oxidized complexes exhibit subtle differences in electronic structure and interaction with exogenous ligands when compared with the oxidized 5-membered chelate backbone **1,2-Salcn** and **Salen** complexes.[20,21] The oxidized **Salpn** complexes exhibit more localized phenoxyl radical species, and the Pd analogue demonstrated localization of the phenoxyl radical on one of the two phenolate moieties and consequently an unsymmetrical coordination environment.[20,21]

Oxidation of the copper salen derivative Cu(**1,2-Salcn**) results in a high-valent, diamagnetic Cu(III) species in the solid state. In solution, however, a temperature-dependent equilibrium exists between a Cu(III)-ligand and a Cu(II)-ligand radical form, indicating the nearly isoenergetic nature of these two species.[22] The shift of the oxidation locus from the ligand for $[Ni(\mathbf{1,2\text{-}Salcn})]^+$ to the metal for $[Cu(\mathbf{1,2\text{-}Salcn})]^+$ matches the trend for the monoanionic Ni- and Cu-dithiolenes.[23] For Ni(**1,2-Salcn**), the redox-active orbitals of the ligand are positioned at a higher energy in comparison with the d-orbital manifold, resulting in ligand oxidation to form $[Ni(\mathbf{1,2\text{-}Salcn})]^+$.[19,21] For Cu(**1,2-Salcn**), occupancy of the higher energy metal-centered orbital ($d_{x^2-y^2}$) results in a Cu(III) complex upon oxidation.[22] On the other hand, Thomas et al. have reported that a *para*-methoxy substituted phenolate derivative of Cu(**1,2-Salcn**) yields a partially localized Cu(II)-phenoxyl radical complex upon oxidation.[24]

In this paper, we report the synthesis of the one-electron oxidized Cu(**1,3-Salcn**) complex (**1,3-Salcn** = *N,N′*-bis(3,5-di-*tert*-butylsalicylidene)-1,3-cyclohexanediamine (Figure 2) and characterization of the physical properties and reactivity in comparison with **1,2-Salcn** analogues. The **1,3-Salcn** ligand has the same N_2O_2 donor set as that of the previously studied **Salen** and **1,2-Salcn** analogues but contains a six-membered chelate ring. We expected that the 6-membered chelate backbone would lead to coordination plane distortion and that this structural change would influence the orbital overlap between the copper ion and the ligand as seen for the group 10 metal **Salpn** complexes.[20] Our results show that the oxidized 6-membered chelate complex can be described as a Cu(II)-phenoxyl radical species, which differs from the Cu(III)-phenolate ground state determined for one-electron oxidized Cu(**1,2-Salcn**). By a combination of experiments and calculations we now show that conversion from a 5- to a 6-membered chelate backbone alters the electronic structure of the one-electron oxidized copper(II) complexes. Our reactivity results also show that the Cu(II)-phenoxyl radical species, $[Cu(\mathbf{1,3\text{-}Salcn})]^+$, which exhibits an electronic structure comparable to the oxidized form of GO, is more reactive toward alcohol oxidation as compared to $[Cu(\mathbf{1,2\text{-}Salcn})]^+$.

EXPERIMENTAL SECTION

Materials and Methods. All the chemicals used were of the highest grade available and were further purified whenever necessary.[25] Solvents were also purified before use by standard methods.[25] *N,N′*-bis(3,5-di-*tert*-butylsalicylidene)cyclohexane-1,3-diamine (H_2**1,3-Salcn**) was prepared in a manner similar to the ligands H_2**1,2-Salcn** and H_2**Salen** (Figure 2).[16] UV−vis−NIR spectra were obtained with a JASCO V-670 spectrophotometer, equipped with a liquid nitrogen cooled cryostat, UNISOKU CoolSpeK UV USP-203-A, from −80 to 30 °C. Cyclic voltammetry (CV) was performed on a HOKUTO DENKO HZ-5000 automatic polarization system, equipped with a Ag wire reference electrode, a platinum disk working electrode, and a Pt counter electrode with 0.1 M Bu_4NClO_4 solutions in CH_2Cl_2. Ferrocene was used as an external standard. Electrospray ionization mass spectra (ESI-MS) were collected with a PE Sciex API 300 mass spectrometer. All electron paramagnetic resonance (EPR) spectra were collected using a Bruker EMX plus spectrometer operating with either an X-band or a Q-Band (~34 GHz) microwave bridge. For the X-Band

dx.doi.org/10.1021/ic3018503 | *Inorg. Chem.* 2012, 51, 12450−12461

experiment a dual mode cavity operating both at ~9.6 GHz (for an orientation perpendicular to the magnetic field) and ~9.4 GHz (for an orientation parallel to the magnetic field) was used. Low temperature measurements of frozen solutions were conducted with a Bruker helium temperature-control system and a continuous flow cryostat. Samples for X-band measurements were placed in 4-mm outer-diameter sample tubes with sample volumes of ~400 μL. Samples for Q-band measurements were loaded in 1-mm outer-diameter sample tubes containing sample volumes of ~40 μL. EPR spectra were simulated with a commercial Bruker XSophe software. The X-ray photoelectron spectra (XPS) were recorded on a Thermo VG Scientific Model Theta Probe spectrometer using Al Kα radiation (1486.6 eV) operated at 15 kV and 3 mA as the X-ray excitation source. The solid sample was dispersed on an In film, and the carbon 1s binding energy (284.5 eV) was used to calibrate the binding energy.[26] Resonance Raman spectra were measured with a JASCO NR-1800 triple polychromator equipped with a liquid-nitrogen-cooled Princeton Instruments CCD detector. Raman shifts were calibrated with indene, the accuracy of the peak positions of the Raman bands being ± 1 cm^{-1}.

Synthesis of Complexes. [Cu(1,3-Salcn)] (1). To a solution of H_2**1,3-Salcn** (0.51 g, 1.0 mmol) in CH_2Cl_2 (10 mL) was added $Cu(CH_3COO)_2{\cdot}2H_2O$ (0.21 g, 1.0 mmol) in C_2H_5OH (10 mL). The resulting solution was refluxed for a few minutes and kept standing at room temperature for 2−3 h to afford a brown precipitate. Brown-green crystals were obtained by recrystallization from CH_2Cl_2/MeOH. Elemental analysis (%) calcd for **1** ($C_{36}H_{52}N_2O_2Cu$): C, 71.07; H, 8.62; N, 4.60. Found: C, 70.77; H, 8.62; N, 4.55.

[Cu(1,3-Salcn)]SbF$_6$ ([1]SbF$_6$). To a solution of Cu(**1,3-Salcn**) (**1**) (0.608 g, 1.0 mmol) in CH_2Cl_2 (15 mL) was added $AgSbF_6$ (0.344 g, 1.0 mmol), and after a few minutes the reaction mixture was filtered. A few drops of toluene were added to the resulting solution, which was kept standing overnight below −60 °C to afford green crystals. Elemental analysis (%) calcd for [**1**]**SbF$_6$** ($C_{36}H_{52}N_2O_2CuSbF_6{\cdot}0.25(C_7H_8){\cdot}0.5(CH_2Cl_2)$): C, 50.51; H, 6.09; N, 3.08. Found: C, 50.74; H, 6.26; N 2.99.

[Cu(1,2-Salcn)] (2) and [Cu(1,2-Salcn)]SbF$_6$ ([2]SbF$_6$). These complexes were synthesized according to the literature.[22]

X-ray Structure Determination. The X-ray experiment was carried out on well-shaped single crystals of complex $[\mathbf{1}]^+$ on a Rigaku FR-E CCD area detector with graphite monochromated Mo Kα radiation (λ = 0.71073 Å). The crystals were mounted on a glass fiber. To determine the cell constants and orientation matrix, 6 oscillation photographs were taken for each frame with the oscillation angle of 0.3° and the exposure time of 16 s. Reflection data were corrected for both Lorentz and polarization effects. The structures were solved by the heavy-atom method and refined anisotropically for non-hydrogen atoms by full-matrix least-squares calculations. All the disordered carbons were also refined anisotropically. Each refinement was continued until all shifts were smaller than one-third of the standard deviations of the parameters involved. Atomic scattering factors and anomalous dispersion terms were taken from the literature.[27] All hydrogen atoms were located at the calculated positions and were assigned a fixed displacement and constrained to an ideal geometry with C−H = 0.95 Å. The thermal parameters of calculated hydrogen atoms were related to those of their parent atoms by U(H) = 1.2U_{eq}(C). All the calculations were performed by using the CrystalStructure program package.[28] Summaries of the fundamental crystal data and experimental parameters for structure determination are given in Supporting Information, Table S1.

Kinetic Measurements. Kinetic measurements for the reaction of $[\mathbf{1}]^+$ with benzyl alcohol were carried out on a Shimadzu UV2550 or a JASCO V-660 spectrophotometer. The temperature of the sample solutions was held constant within ±0.1 °C using a thermostatted cell unit. All the sample solutions for UV−vis measurements were prepared using purified CH_2Cl_2. Anhydrous benzyl alcohol (99.8%, Aldrich) was used without further purification. α-Benzyl-d_2 alcohol was synthesized from benzoyl chloride and lithium aluminum deuteride and was used immediately after purification: The reactions are highly sensitive to impurities of the deuterated alcohol as reported in ref 29. Benzyl alcohol-d ($C_6H_5CH_2OD$) was obtained through the H−D exchange between $C_6H_5CH_2OH$ and D_2O, and was confirmed as >80 atom % deuteration by NMR spectroscopy.

The sample solutions for the kinetic measurements were prepared by the following two procedures: (A) A 5.0 mM solution of $[\mathbf{1}]^+$ was prepared by filtering the mixture of 5.0 mM CH_2Cl_2 solution of **1** and 1 equiv of $AgSbF_6$. After the solution of benzyl alcohol in CH_2Cl_2 ($[C_6H_5CH_2OH]$ = 0.1−1.0 M, 2.5 mL) in a 10-mm quartz cell was adjusted to the appropriate reaction temperature, the reaction was initiated by adding 100 μL of the 5.0 mM solution of $[\mathbf{1}]^+$. From this procedure, the total concentration of $[\mathbf{1}]^+$ in the sample solutions was 0.2 mM, which was much lower than that of benzyl alcohol (0.1−1.0 M). (B) After the 0.2 mM solution of $[\mathbf{1}]^+$ in CH_2Cl_2 (2.3 mL) in a 10-mm quartz cell was adjusted to the appropriate reaction temperature, the reaction was initiated by adding the calculated amount of benzyl alcohol directly into the cell. The kinetic data obtained from procedure (A) were in good agreement with those from (B). The kinetic measurements for the reaction with α-benzyl-d_2 alcohol and benzyl alcohol-d (1.0 M) were carried out by procedure (B) using freshly purified alcohol as mentioned above.

The change in the absorbance at 440 nm over time for the reaction of $[\mathbf{1}]^+$ with a large excess benzyl alcohol in CH_2Cl_2 was analyzed with first-order kinetics within at least three half-lives of the decrease of $[\mathbf{1}]^+$. Therefore, the reaction rate was expressed as a pseudo first-order rate law, $-d[[\mathbf{1}]^+]/dt = k_{obs}[[\mathbf{1}]^+]$, where k_{obs} denotes the conditional pseudo first-order rate constant. The k_{obs} values were obtained by applying nonlinear least-squares fitting of $A_t = A_\infty + (A_0 - A_\infty)\exp(-k_{obs}t)$ to the data of absorbance change with time, where A_0, A_t, and A_∞ denote the absorbances at the reaction time, t = 0, t, and infinite time, respectively.

Calculations. Geometry optimizations were performed using the Gaussian 09 program (Revision A.02),[30] the CAM-B3LYP[31,32] functional, and the 6-31G(d) basis set on all atoms. Broken-symmetry[33] (BS) density functional theory (DFT) calculations were performed with the same functional and basis sets. Frequency calculations at the same level of theory confirmed that the optimized structures were located at a minimum on the potential energy surface. Single point calculations were performed using the CAM-B3LYP[31,32] functional and the TZVP basis set of Ahlrichs[34] on all atoms. The above calculations were also completed using the B3LYP[35,36] functional for comparison. AOMix[37] was used for determining atomic orbital compositions employing Mulliken Population Analysis. The intensities of the 30 lowest-energy electronic transitions were calculated by TD-DFT[38] with a polarized continuum model (PCM) for CH_2Cl_2 (dielectric ε = 8.94).[39]

RESULTS

Characterization and Redox Behavior of Cu(1,3-Salcn) (1). The 6-membered chelate N_2O_2-donor ligand H_2**1,3-Salcn** (Figure 2) reacted with copper(II) acetate in C_2H_5OH to give Cu(**1,3-Salcn**) (**1**) as brownish-green crystals. The absorption spectrum of complex **1** showed typical bands for a copper(II)-salen type complexes at 623 (ε = 460 M^{-1} cm^{-1}) and 387 nm (ε = 15500 M^{-1} cm^{-1}). In comparison with complex Cu(**1,2-Salcn**) (**2**), these bands were slightly red-shifted from 569 (ε = 600 M^{-1} cm^{-1}) and 377 (ε = 11600 M^{-1} cm^{-1}), respectively.[22] The intensity of the 623 nm band of **1** was lower, while that of the 386 nm band was higher. Such intensity differences are also observed for the group 10 metal 5- and 6-membered salen type complexes.[20] These spectral differences for **1** in comparison to **2** are likely due to the 6-membered chelate effect. The cyclic voltammogram of **1** showed two reversible redox waves at $E_{1/2a}$ = 0.48 and $E_{1/2b}$ = 0.63 V vs Fc/Fc$^+$ in the range of 0−1.0 V (Figure 3). The potentials were only 0.03 V higher than those of complex **2**, and these redox waves were found to be one electron processes from the current analysis for each wave.[22] This result suggests that one-electron oxidized complex **1** can

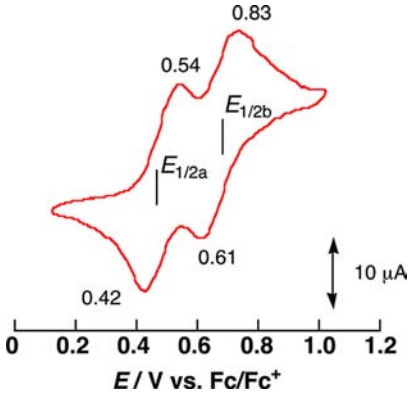

Figure 3. CV of complex **1** in CH_2Cl_2.

be generated by adding an equimolar amount of chemical oxidants such as $AgSbF_6$, which have also been used for oxidation of complex **2**.[40] Indeed, the addition of an equimolar amount of $AgSbF_6$ to **1** in CH_2Cl_2 caused a color change to dark green, indicating formation of $[\mathbf{1}]^+$. The ESI-mass spectrum of the dark green species exhibited a peak at m/z = 608, and in combination with further characterization results (vide infra), the one-electron oxidized complex, $[\mathbf{1}]^+$, can be described as a monocationic species, $[Cu(\mathbf{1,3\text{-}Salcn})]^+$.

Crystal Structure and Solid State Characterization of [Cu(1,3-Salcn)]SbF_6 ([1]SbF_6). When the dark green solution of $[\mathbf{1}]^+$ prepared by $AgSbF_6$ oxidation was kept below −60 °C overnight in CH_2Cl_2/toluene, green crystals of the one-electron oxidized **1,3-Salcn** complex, $[\mathbf{1}]\mathbf{SbF_6}$, could be isolated. The X-ray crystal structure analysis gave the structure of $[\mathbf{1}]\mathbf{SbF_6}$, whose ORTEP view is shown in Figure 4. The structure of

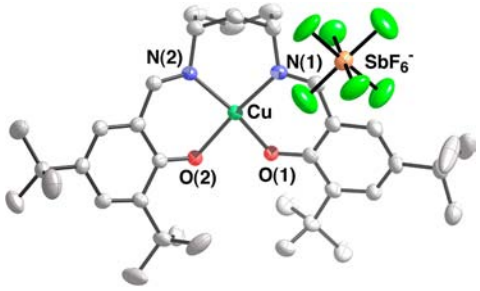

Figure 4. ORTEP view of Cu(II)-phenoxyl radical complex, $[\mathbf{1}]\mathbf{SbF_6}$.

complex $[\mathbf{1}]^+$ exhibits a pseudo square-planar geometry formed by two phenolato oxygen atoms and two imino nitrogen atoms. The Cu coordination sphere geometry is asymmetric, indicating that one salicylideneimino moiety becomes a weaker donor in $[\mathbf{1}]^+$ with a longer bond to Cu (Cu−O(1) 1.996(3) vs Cu−O(2) 1.912(3) Å). The C−O bond length of the weakly donating phenolate moiety is shortened (1.266(5) Å), and the ring *ortho*-C−C bonds are lengthened (1.443(6) and 1.422(6) Å). This quinoid bonding pattern is consistent with radical localization to one side of the molecule in $[\mathbf{1}]^+$, in agreement with the bonding pattern observed for other localized phenoxyl radical complexes.[18−21,24,41,42] In addition, the SbF_6^- counter-ion was located close to the quinoid moiety in $[\mathbf{1}]^+$; the closest distance was 3.026 Å between the SbF_6^- and the C−O carbon atom of the phenoxyl ligand. Association of the counterion with the phenoxyl ligand was also observed in other unsymmetric M(II)-phenoxyl radical salen-type complexes.[20,24]

Previously, we have reported that the 6-membered chelate group 10 metal **Salpn** complexes showed a more distorted geometry as compared with the **1,2-Salcn** and **Salen** analogues, with larger angles between the two cis N−M−O planes in the **Salpn** complexes.[20] In the case of the oxidized copper(II) complexes, we did not observe a large distortion of the 6-membered chelate **1,3-Salcn** complex in comparison with the 5-membered chelate **1,2-Salcn** complex. For example, the angle between the N−Cu−O planes in a cis configuration was estimated to be 12.7°, which is smaller than the distortion in the 6-membered diimine chelate complex $[Ni(\mathbf{Salpn})]SbF_6$ (21.4°)[20] and neutral 5-membered diimine chelate complex **2** (19.8°).[22] This may be due to the rigidity of the cyclohexanediamine moiety. However, we have not been able to completely determine the crystal structure of precursor complex **1**, mainly because of difficulties in the determination of space group, and therefore, direct comparison of $[\mathbf{1}]\mathbf{SbF_6}$ with neutral complex **1** could not be made. The structure of complex **1** obtained at this stage is shown in the Supporting Information, Figure S1.

On the other hand, angles between the two phenolate planes of complex $[\mathbf{1}]^+$ were estimated to be 41.7(1)°, which is larger than other 6-membered chelate phenoxyl radical complexes. For comparison, the angles between the two phenolate planes in group 10 metal **Salpn** complexes were estimated to be 28.3° for $[Ni(\mathbf{Salpn})]^+$, 24.1° for $[Pd(\mathbf{Salpn})]^+$, and 18.0° for $[Pt(\mathbf{Salpn})]^+$, whose values are smaller than the angle for $[\mathbf{1}]^+$. The large distortion of these two phenolate moieties in $[\mathbf{1}]^+$ from the square plane may lead to the localized electronic structure because of limited orbital overlap and the associated effect on radical electron communication through the central copper ion.

XPS analysis of the Cu $2p_{3/2}$ and $2p_{1/2}$ binding energies was used for assessing the metal oxidation state for the neutral and one-electron oxidized **1,3-Salcn** complexes in the solid state (Supporting Information, Figure S2). The XPS values depend on the oxidation state of the metal ion, and for the analogous complex **2**, the energy differences between the Cu(II) and Cu(III) oxidation states have been reported to be about +1.2 eV for both $2p_{1/2}$ and $2p_{3/2}$ binding energies.[22] The XPS values for **1** and $[\mathbf{1}]^+$ are very similar ($2p_{3/2}$ = 933.7 and $2p_{1/2}$ = 953.6 eV for **1** and $2p_{3/2}$ = 933.7 and $2p_{1/2}$ = 953.7 eV for $[\mathbf{1}]^+$), and $[\mathbf{1}]^+$ is therefore assigned as a Cu(II)-ligand radical species.

Magnetic Properties. The magnetic properties of $[\mathbf{1}]^+$ have been investigated by multifrequency EPR and temperature dependent magnetic susceptibility. The 12 K X-band EPR spectra of a frozen CH_2Cl_2 solution of $[\mathbf{1}]^+$ have been recorded both in perpendicular and parallel modes. The perpendicular mode spectrum exhibited very broad signals at about g = 4 and g = 1.5 assigned to spin triplet (S = 1) resonances with a mononuclear Cu(II) signal at g = 2 (Supporting Information, Figure S3) arising from about 5% of neutral complex **1** as a contaminant in the sample. The very broad EPR signals and distribution over a large magnetic field suggests that the zero field splitting parameters are within the range of or slightly larger than the X-band energy (∼ 0.3 cm^{-1} at ν = 9.4 GHz).[43] Therefore, the spectrum is not satisfactory for accurate determination of the zero-field splitting parameters.[44] On the other hand, the parallel mode is particularly useful for characterizing integer electron spin systems as it allows for greater intensity of the forbidden transitions.[45] The parallel mode X-Band EPR spectrum exhibited a dominant transition at $g \sim 4$ assigned to the $\Delta M_S = \pm 2$ transition, which further

dx.doi.org/10.1021/ic3018503 | *Inorg. Chem.* 2012, 51, 12450−12461

confirms an accessible triplet spin state of $[\mathbf{1}]^+$. The intensity of the EPR spectrum was studied as a function of temperature: An increase of the intensity of the spin triplet signals was observed upon decreasing the temperature, suggesting weak ferromagnetic coupling between the ligand radical and the copper spins.

To gain insight into the zero field splitting parameters, we conducted EPR measurements at a higher frequency (Q-Band, $\nu \sim 34$ GHz) on a frozen CH_2Cl_2 solution of $[\mathbf{1}]\mathbf{SbF_6}$.[46] The Q-Band spectrum at 12 K clearly consists of a two-line pattern centered at $g = 2.06$, as well as a half-field $\Delta M_S = \pm 2$ transition at $g = 4$ (Figure 5). This signature is characteristic of a spin

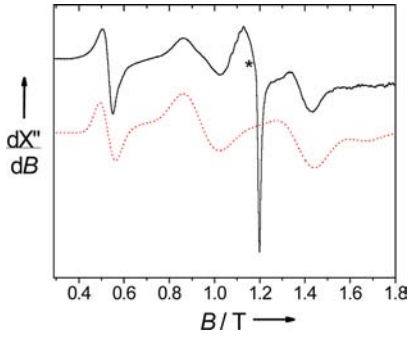

Figure 5. Q-Band EPR spectrum of a frozen 0.02 M CH_2Cl_2 solution of $[\mathbf{1}]\mathbf{SbF_6}$: The solid black line is the experimental spectrum, and the dotted red line is a simulation of the triplet system using the parameters given in the text. The asterisk denotes a paramagnetic mononuclear copper ($S = 1/2$) impurity present in the sample. Modulation Frequency 100 kHz, amplitude 0.5 mT, microwave power 1.5 mW, frequency 34.02 GHz, $T = 12$ K.

triplet system having zero field splitting (ZFS) parameters smaller than the Q-Band energy quantum ($\sim$1.1 cm^{-1}).[47] The spectrum could be satisfactorily simulated by using the ZFS parameters $|D| = 0.470 \pm 0.035$ cm^{-1}, $E/D = 0.06 \pm 0.02$ and $g_{iso} = 2.06$. We additionally used these parameters to simulate the X-Band spectra and found a reasonable agreement with the experimental data (see Supporting Information, Figure S3). From these EPR results, the triplet spin state of a Cu(II)-phenoxyl salen complex could be evidenced experimentally. The ZFS parameters reported here are the first measured experimentally for Cu(II)-phenoxyl salen complexes.

The temperature dependent magnetic susceptibility of $[\mathbf{1}]\mathbf{SbF_6}$ in the solid state exhibited a decrease in the susceptibility as the temperature was lowered. Consideration of only the intramolecular interaction leads to the fitting of this plot as a weak antiferromagnetic $S = 0$ ground state with the exchange coupling $J/k_B = -1.9$ cm^{-1} based on $\boldsymbol{H} = -2J\boldsymbol{S}_{Cu}\cdot\boldsymbol{S}_{rad}$. This fitting is contradictory to the result of EPR experiments. Final fitting of the temperature dependent magnetic susceptibility was based on the Bleaney–Bower's equation[48] considering the ZFS values:[49]

$$\chi = \frac{2Ng^2\beta^2}{k_B T[2 + \exp(D/k_B) + \exp(-2J/k_B(T-\theta))]} \quad (1)$$

The best-fit parameters are $J/k_B = 4.1$ cm^{-1} and $\theta = -3.4$ cm^{-1} using the values from the results of EPR measurements, $g = 2.06$ and $D/k_B = 0.47$ cm^{-1} (Figure 6). These results indicate that the intramolecular interaction between copper and radical unpaired electron spins (J/k_B) is ferromagnetic, while the intermolecular interaction (θ) is weakly antiferromagnetic. This intramolecular coupling value matches with the EPR experiments. Thus, complex $[\mathbf{1}]^+$ can be assigned to a Cu(II)-phenoxyl radical species with a $S = 1$ ground state exhibiting a weak ferromagnetic interaction between the Cu(II) center and the ligand radical.

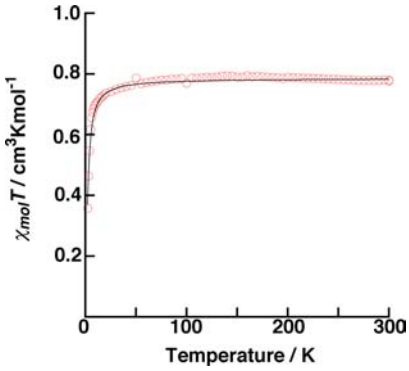

Figure 6. Temperature dependent magnetic susceptibility of $[\mathbf{1}]\mathbf{SbF_6}$. Red dots are actual measurements, black line is fitting based on the Bleaney–Bower's equation.

Theoretical Characterization. Density functional theory (DFT) calculations of **1** and $[\mathbf{1}]^+$ were completed using both the B3LYP[36] and the Coulomb-Attenuated Method (CAM-B3LYP)[31,32] functionals. With the use of the B3LYP functional the metrical parameters for **1** were reproduced within $\pm$0.02 Å (Supporting Information, Table S2). However, the B3LYP functional predicted an essentially symmetric complex for $[\mathbf{1}]^+$, in contrast to the experimental metrical parameters. We thus employed CAM-B3LYP, as this functional has been demonstrated to be useful for predicting the energies of delocalized systems,[50] as well as long–range charge transfer transitions.[51] In the CAM approach the exchange interaction at short-range is modeled with 0.19 Hartree–Fock (HF) and 0.81 Becke 1988 (B88), while the long–range interaction is modeled with 0.65 HF and 0.35 B88. The intermediate region is described by a standard error function.[31] The triplet and broken symmetry calculations (vide infra) for $[\mathbf{1}]^+$ using the CAM-B3LYP functional both predicted a large asymmetry in the coordination sphere, in good correspondence with the X-ray data (Table 1). The predicted Cu–O phenoxyl bond (Cu–O(1)) length closely matches the X-ray data, and a phenoxyl bonding pattern is evident in the C–O and ring C–C bonds. The predicted Cu–O phenolate bond (Cu–O(2)) is shorter than the experimental value (1.84 Å vs 1.912 Å), which could be attributed to the localizing effect of the CAM-B3LYP functional.[52] Overall, we have found that the CAM-B3LYP functional predicts the asymmetric geometric structure for $[\mathbf{1}]^+$, and in addition, matches the experimental data in terms of the electronic structure.

The energies of the high spin triplet ($S = 1$) and broken symmetry ($S = 0$) electronic states for $[\mathbf{1}]^+$ were calculated and compared to the experimental magnetic data (vide infra). The high spin triplet solution was determined to be favored by only 0.6 kcal mol^{-1}, matching both the experimental ground state and the small energy difference determined by solid state magnetism and EPR. The closed-shell singlet state was determined to be 18 kcal mol^{-1} higher in energy in comparison to the triplet ground state. The spin density distribution for both the triplet and the broken symmetry solutions (Figure 7) shows localization of the ligand radical on one side of the ligand framework in accordance with the experimental data. In contrast, a delocalized ligand radical structure is predicted if

dx.doi.org/10.1021/ic3018503 | Inorg. Chem. 2012, 51, 12450–12461

Table 1. Experimental and Calculated (CAM-B3LYP) Coordination Sphere Metrical Parameters for Complexes 1 and $[1]^+$ in Å

compound and method	Cu−O(1)	Cu−O(2)	Cu−N(1)	Cu−N(2)	C−O
1	1.895	1.891	1.955	1.962	1.295/1.298
$[1]^+$ (X-ray)	1.995	1.912	2.006	1.963	1.265/1.304
$[1]^+$ triplet	1.987	1.842	1.982	1.925	1.259/1.311
$[1]^+$ broken symmetry	1.993	1.841	1.922	1.983	1.257/1.311

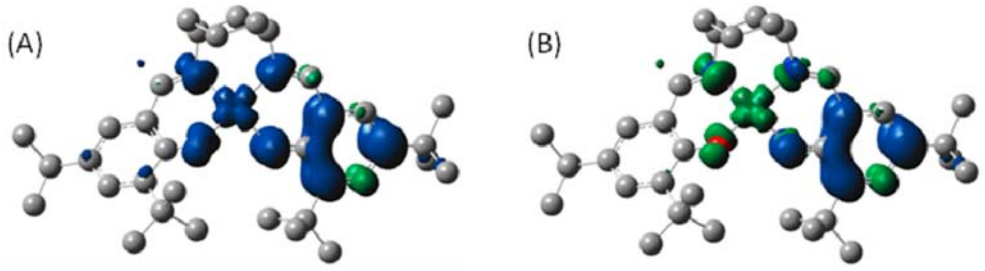

Figure 7. Spin density plots for $[1]^+$ showing localization of the ligand radical on one side of the ligand framework; (A) triplet and (B) broken symmetry solutions.

the B3LYP functional is employed (Supporting Information, Figure S4). A typical phenoxyl radical spin density pattern is observed for the CAM-B3LYP calculations with positive spin population at the $O_{phenoxyl}$ (0.31), C_{ortho} (0.23, 0.33), and C_{para} (0.42) positions of one ring (Figure 7**A**).

Absorption and Resonance Raman Spectroscopy. The UV−vis−NIR absorption spectrum of $[1]^+$ in CH_2Cl_2 exhibits characteristic new bands at λ (ε/M^{-1} cm^{-1}) = 29900 (8550), 26000 (7700), 22800 (4550), 19600 (650), 16100 (610), 11900 (920), and 6600 (920) cm^{-1} (Figure 8). The absorption spectral features especially of the NIR bands are different from those of complex $[2]^+$. The NIR bands of $[1]^+$ are of significantly lower intensity compared to the NIR transitions for the Cu(III) ground state complex $[2]^+$, which exhibited intense visible 18600 (6500) and NIR 5600 cm^{-1} (2900) LMCT bands.[22] Further, the characteristic 22800 cm^{-1} band can be ascribed to the $\pi-\pi^*$ transition of the coordinated phenoxyl radical.[11−13,53,54] Therefore, the absorption spectral features of $[1]^+$ clearly suggest that complex $[1]^+$ is a Cu(II)-phenoxyl radical species in solution.

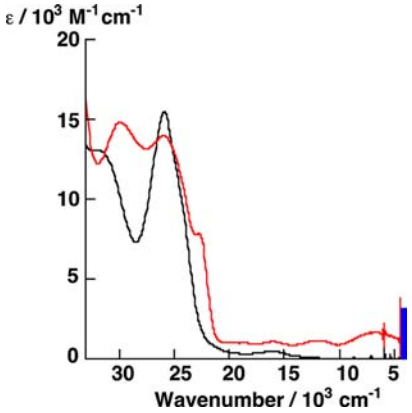

Figure 8. UV−vis−NIR spectra of complexes **1** and $[1]^+$ in CH_2Cl_2: Black line, complex **1**; red line, complex $[1]^+$. The vertical blue line at low energy corresponds to the calculated low energy transition at 3790 cm^{-1} for $[1]^+$ (triplet).

We have previously examined the shape and intensity of the visible and NIR bands of the oxidized group 10 metal(II) and Cu(II) salen type complexes to assess the degree of coupling between the redox-active phenolates.[18−22,55] The oxidized group 10 metal **1,2-Salcn**, **Salen**, and **Salpn** complexes were assigned to fully delocalized Class III or Class II/III borderline systems,[18,20,21] based on the Robin−Day classification system.[56−58] Class III systems exhibit intervalence transitions (IVCT) that are characteristically intense ($\varepsilon_{max} \geq 5000$ M^{-1} cm^{-1}) and narrow (bandwidths ($\Delta\upsilon_{1/2}$) ≤ 2000 cm^{-1}) and are solvent independent.[59] The NIR band intensity of the Cu(II)-phenoxyl radical complex $[1]^+$ at 6600 cm^{-1} (ε_{max} = 920 M^{-1} cm^{-1}, $\Delta\upsilon_{1/2}$ = 1430 cm^{-1}) is much lower and the bandwidth is larger than the values for the Class III systems of group 10 metal salen-type complexes.[20,21] The minimum bandwidth of complex $[1]^+$ in the high-temperature limit predicted from eq 2[58−60] can be estimated to be $\Delta\upsilon_{HTL}$ = 3910 cm^{-1}, which is larger than the experimental value of $\Delta\upsilon_{1/2}$ = 1430 cm^{-1}:

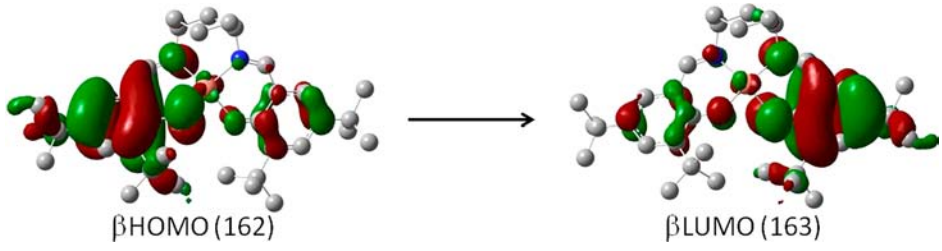

Figure 9. TD-DFT assignment of the calculated low energy transition for $[1]^+$ (triplet). The predicted βHOMO → βLUMO transition is assigned as a ligand-to-ligand charge transfer (LLCT) band in accord with the Class II intervalence description in the text.

dx.doi.org/10.1021/ic3018503 | Inorg. Chem. 2012, 51, 12450−12461

$$\Delta\upsilon_{HTL} = \sqrt{16 \ln 2RT\upsilon_{max}} \quad (2)$$

Furthermore, the shift in the band energy (ε_{max}) between toluene and CH_2Cl_2 was about 800 cm^{-1} (Supporting Information, Figure S5, Table S3), which is 10-fold larger than that of the class III fully delocalized complex [Pt(**Salen**)]$^+$.[21] Experimental analysis of complex [**1**]$^+$ demonstrates that this derivative is best described as a Class II intervalence complex.

We used time-dependent DFT (TD-DFT)[38] to better understand the origin of the low energy NIR transition for [**1**]$^+$. The predicted band with highest intensity for the triplet ground state was red-shifted in comparison to the experimental data (Figure 8), but provides information on the nature of this transition. The predicted band is predominantly a βHOMO → βLUMO transition (Figure 9), and is assigned as a phenolate to phenoxyl intervalence charge transfer (IVCT) transition in accord with the Class II description for [**1**]$^+$.

The resonance Raman spectrum (Figure 10) of complex [**1**]$^+$ exhibited characteristic new intense bands at 1494 cm^{-1} and

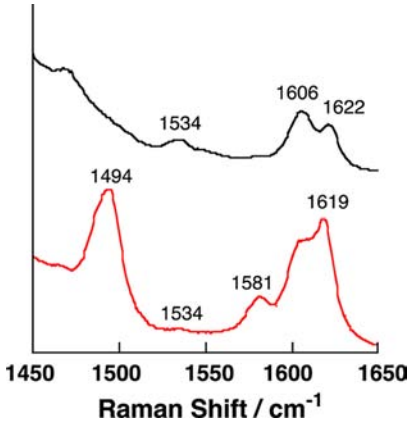

Figure 10. Resonance Raman spectra of complexes **1** and [**1**]$^+$ (λ_{ex} = 413.1 nm) in CH_2Cl_2 at −60 °C: Black line, complex **1**; red line, complex [**1**]$^+$.

1581 cm^{-1}, which can be assigned to the phenoxyl radical ν_{7a} and ν_{8a} bands, respectively.[11,61] On the other hand, the phenolate ν_{11a} band at 1534 cm^{-1} was also observed but is very weak, and the 1606 cm^{-1} band remained in the spectrum of [**1**]$^+$. The very weak 1534-cm^{-1} band intensity may be due to the different enhancement from resonance Raman of the neutral species. These results support that one-electron oxidized complex [**1**]$^+$ is a Cu(II)-phenoxyl radical that can be described as having an asymmetric coordination structure (phenolate and phenoxyl moieties), which is in good agreement with the NIR spectral data.[19]

Reactivity of the Oxidized 1,3-Salcn Complex with Benzyl Alcohol. A CH_2Cl_2 solution of the localized phenoxyl radical complex [**1**]$^+$ is relatively stable at 293 K, with a decay constant of less than 1.5×10^{-5} s^{-1} for 0.1−0.3 mM solutions, the half-life of [**1**]$^+$ being estimated to be longer than 13 h. Addition of excess benzyl alcohol to a solution of [**1**]$^+$ in CH_2Cl_2 caused a color change to bright green within one hour. GC-MS and absorption spectral changes revealed that formation of the benzaldehyde was in 50% yield relative to the initial amount of the phenoxyl radical complex. This reaction was also observed under a nitrogen atmosphere, indicating that the presence of air did not affect the benzyl alcohol oxidation. The UV−vis absorption spectral change revealed that the spectrum of the final product is different from that of complex **1**, since the final product has weak visible bands at about 500 and 600 nm (Figure 11). Addition of 1 equiv of

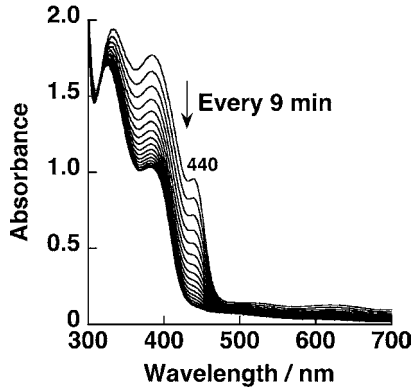

Figure 11. Absorption spectral changes with time for the reaction of complex [**1**]$^+$ (0.2 mM) with benzyl alcohol (0.1 M) in CH_2Cl_2 at 293 K. The spectra were recorded at 9 min intervals.

Et_3N to the solution of the final product affords a spectrum similar to complex **1**, indicating that the final product of this reaction can be assigned to the proton adduct of the Cu(II) complex, [**1H**]$^+$. The ESI-MS spectrum of the final product supported the existence of the proton adduct [**1H**]$^+$ with the observation of m/z = 609. The overall stoichiometry of the reaction observed is expressed as follows:

$$2[Cu(\mathbf{1}, \mathbf{3\text{-}salcn^{\bullet}})]^+ + C_6H_5CH_2OH \rightarrow 2[Cu(H\mathbf{1}, \mathbf{3\text{-}salcn})]^+ + C_6H_5CHO \quad (3)$$

The reaction stoichiometry of complex [**1**]$^+$ with benzyl alcohol is in good agreement with that of complex [**2**]$^+$ reported previously.[29]

In the presence of a large excess of benzyl alcohol, conversion of [**1**]$^+$ to [**1H**]$^+$ can be regarded as a first-order process, suggesting that only one molecule of complex [**1**]$^+$ is involved in the rate-determining step.[29] The first-order decay constant (k_{obs}) of complex [**1**]$^+$ was not changed by varying the concentration of complex (k_{obs} = (3.61−4.06) × 10^{-3} s^{-1} for 0.1−0.3 mM solution of [**1**]$^+$ at [$C_6H_5CH_2OH$] = 1.0 M, Supporting Information, Table S4), while the rate constant depended on the benzyl alcohol concentration. A plot of k_{obs} against the concentration of benzyl alcohol exhibited a linear correlation (Supporting Information, Figure S6), that is, $k_{obs} = k_2[C_6H_5CH_2OH]$, giving the second-order rate constant k_2 = (3.89 ± 0.05) × 10^{-3} M^{-1} s^{-1} at 293 K for the rate-determining process. We could not determine the association constant of complex [**1**]$^+$ with benzyl alcohol because of the linear correlation. The reactivity characteristics are very similar to the reaction of complex [**2**]$^+$ with benzyl alcohol, although the second-order rate constant of [**1**]$^+$ is about 4 times larger than that of complex [**2**]$^+$ (k_2 = 1.02 × 10^{-3} M^{-1} s^{-1} at 293 K was obtained at [$C_6H_5CH_2OH$] = 1.0 M, Supporting Information, Table S4). From the kinetic analyses, the primary alcohol oxidation by phenoxyl radical complex [**1**]$^+$ likely occurs by a mechanism similar to that of [**2**]$^+$ but with a faster reaction rate.[29]

To determine whether C−H bond cleavage is involved in the rate determining step, we carried out kinetic analyses using α-

dx.doi.org/10.1021/ic3018503 | Inorg. Chem. 2012, 51, 12450−12461

benzyl-d_2 alcohol. Previously the kinetic isotope effect (KIE), $k_2(H)/k_2(D)$, for complex $[2]^+$ has been reported to be 19 at 298 K, and the same value was also obtained at 293 K from our measurements.[29] In this study, the KIE value of complex $[1]^+$ was estimated to be 13 at 293 K, which indicates that the C−H bond scission is included in the rate-determining step. On the other hand, the reaction rate for $C_6H_5CH_2OD$ was very similar ($k_2 = 3.6 \times 10^{-3}$ M^{-1} s^{-1} obtained at $[C_6H_5CH_2OD] = 1.0$ M, Supporting Information, Table S4) to that of $C_6H_5CH_2OH$, indicating that the benzyl alcohol oxidation proceeds without the O−H hydrogen abstraction, in the rate determining step. These observations are in line with general hydrogen abstraction from alcohols: Hydrogen abstractors react with alcohols (RCH_2OH) to give a hydroxyalkyl radical such as $R\dot{C}HOH$ rather than the alkoxyl radical ($RCH_2O^{\bullet}$), because the alcohol O−H bond is usually stronger than the C−H bonds in the same molecule.[62] The difference of the C−H hydrogen abstraction properties between $[1]^+$ and $[2]^+$ can be estimated from the KIE values. The correlation between KIE and the activation energy difference between C−H and C−D bonds (ΔE_a^{KIE}) is expressed by the following equation:[63]

$$KIE = \frac{k_H}{k_D} = \exp\left[\frac{\Delta E_a^{KIE}}{2RT}\right] \quad (4)$$

Therefore, the activation energy difference between $[1]^+$ and $[2]^+$ ($\Delta(\Delta E_a^{KIE})$) can be estimated according to the following equation:

$$\Delta(\Delta E_a^{KIE}) = 2RT[\ln(KIE_{[2]+}) - \ln(KIE_{[1]+})] \quad (5)$$

From this equation, $\Delta(\Delta E_a^{KIE})$ was calculated to be 0.4 kcal mol^{-1} at 293 K.

As a further step toward a detailed mechanism of benzyl alcohol oxidation by Cu(II)-phenoxyl radical complex $[1]^+$, temperature dependence studies were carried out. The Eyring plots of complexes $[1]^+$ and $[2]^+$ showed linear fits with similar slopes (Figure 12). The activation parameters of $[2]^+$ were

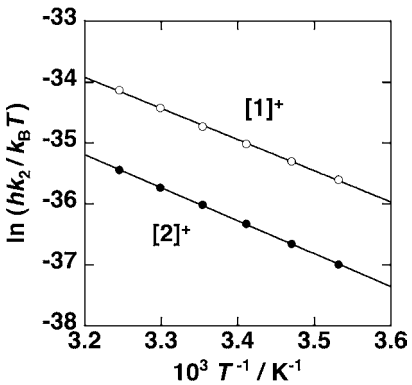

Figure 12. Eyring plots of the second-order rate constants (k_2) for the reactions of complex $[1]^+$ (open circle) and $[2]^+$ (solid circle) with benzyl alcohol. The k_2 values were directly obtained from the k_{obs} at $[C_6H_5CH_2OH] = 1.0$ M at each reaction temperature.

determined to be $\Delta H^{\ddagger} = 10.7 \pm 0.1$ kcal mol^{-1} and $\Delta S^{\ddagger} = -35.6 \pm 0.3$ cal mol^{-1} K^{-1} (Table 2), which are in very good agreement with the reported values ($\Delta H^{\ddagger} = 11.1 \pm 0.4$ kcal mol^{-1} and $\Delta S^{\ddagger} = -34 \pm 1$ cal mol^{-1} K^{-1}).[29] The activation parameters of $[1]^+$ were estimated to be $\Delta H^{\ddagger} = 10.2 \pm 0.1$ kcal mol^{-1} and $\Delta S^{\ddagger} = -34.8 \pm 0.5$ cal mol^{-1} K^{-1}, which are slightly different from those of $[2]^+$ (Table 2). The difference of the activation energy (ΔE_a) between $[1]^+$ and $[2]^+$ is estimated to be 0.6 ± 0.2 kcal mol^{-1} at 293 K. This value is in good agreement with the C−H activation energy difference estimated from the KIE values ($\Delta(\Delta E_a^{KIE}) = 0.4$ kcal mol^{-1}). Thus, the activation parameter difference between $[1]^+$ and $[2]^+$ is relatively small, suggesting a similar reaction mechanism for $[1]^+$ and $[2]^+$, while the C−H hydrogen abstraction by $[1]^+$ is slightly preferred as compared with complex $[2]^+$.

Table 2. Activation Parameters for the Reaction of $[1]^+$ or $[2]^+$ with Benzyl Alcohol

Complex	$\Delta H^{\ddagger}$ kcal mol^{-1}	$\Delta S^{\ddagger}$ cal mol^{-1} K^{-1}	E_a[a] kcal mol^{-1}
$[1]^+$	10.2 ± 0.1	−34.8 ± 0.5	10.8 ± 0.2
$[2]^+$	10.7 ± 0.1	−35.6 ± 0.3	11.3 ± 0.1
	11.1 ± 0.4[b]	−34 ± 1[b]	11.7

[a]Determined from Arrhenius analyses. [b]Ref 29.

DISCUSSION

Metal complexes of tetradentate N_2O_2 Schiff-base ligands, **Salen** and derivatives, have been extensively studied as catalysts for small molecule transformations. Alteration of both the diamine backbone and the substituents on the coordinated phenolate moieties allows the fine-tuning of catalyst activity. Installation of chirality into salen systems via the diamine backbone has resulted in the development of efficient catalysts for a number of important transformations including asymmetric epoxidation and asymmetric epoxide ring-opening reactions. The Cu complex of a tetradentate Schiff-base ligand containing a dinapthylamine backbone exhibited superior alcohol oxidation activity in comparison to the 1,2-cyclohexanediamine analogue.[64] On the other hand, we have previously reported that the one-electron oxidized Cu(**1,2-salcn**) species is a Cu(III)-phenolate in the solid state, while in a CH_2Cl_2 solution it exists in an equilibrium between Cu(III)-phenolate and Cu(II)-phenoxyl radical species.[22] The difference in catalytic activity was attributed to the increased flexibility of the dinapthylamine backbone, affording access to the Cu(I) oxidation state in the catalytic cycle.[64] In this work we have investigated the effects of changing the **Salcn** diamine backbone from 1,2-diamino- (five-membered chelate) to 1,3-diaminocyclohexane (six-membered chelate) on the electronic structure and reactivity of the one-electron oxidized copper(II) bis-Schiff-base complexes.

The copper(II) **1,3-Salcn** complex (**1**) was synthesized by a procedure similar to that for the **Salen** complexes. The redox potential of complex **1** was about 30 mV higher than that of **1,2-Salcn** complex (**2**), the difference being smaller in comparison with the difference of more than 50 mV between 5-membered and 6-membered chelate group 10 metal complexes.[20,21] Therefore the one-electron oxidized copper(II) **1,3-Salcn** complex $[1]^+$ can be generated by addition of 1 equiv of $AgSbF_6$, a method similar to that employed for formation of complex $[2]^+$.

On the basis of the molecular structure determined for crystals of $[1]SbF_6$ suitable for X-ray analysis, the changes in bonding associated with ligand oxidation in the solid state were investigated. The Cu−N bond lengths increased upon oxidation of **1**, while the Cu−O bonds became asymmetric and lengthened slightly on average. The asymmetry is also apparent in the C−O bonds, with the shorter C−O bond on the same side of the molecule as the longer Cu−O bond. This

dx.doi.org/10.1021/ic3018503 | Inorg. Chem. 2012, 51, 12450−12461

bonding pattern is in good agreement with the structures of an oxidized Pd(II) salen complex and other reported localized phenoxyl radical complexes, reflecting the diminished electron-donating ability of the phenoxyl ligand compared with that of the phenolate ligand.[20,21] The SbF_6^- counterion is associated with the phenoxyl ligand in the solid state structure of $[\mathbf{1}]^+$. The asymmetry of the Cu−O bonds for $[\mathbf{1}]^+$ differs from the observed symmetric contraction of the M−O bonds for oxidized Ni and Pt complexes, and can be attributed to diminished delocalization of the li; and radical for $[\mathbf{1}]^+$.[19−21] In comparison to the Cu(III)-phenolate ground state complex $[\mathbf{2}]^+$, $[\mathbf{1}]^+$ shows different Cu−O, Cu−N, and C−O bond lengths and distortion of the coordination plane. The X-ray crystal structure of complex $[\mathbf{2}]^+$ revealed the shortening of these bond lengths, and the angle between the two cis N−Cu−O planes is substantially reduced from that of the neutral complex **2**.[22] These structural differences between $[\mathbf{1}]^+$ and the Cu(III) complex $[\mathbf{2}]^+$ also support that complex $[\mathbf{1}]^+$ is a localized Cu(II)-phenoxyl radical complex.

The phenoxyl radical complex $[\mathbf{1}]^+$ was investigated by a variety of spectroscopic techniques. The XPS of complex $[\mathbf{1}]^+$ exhibited similar Cu $2p_{1/2}$ and $2p_{3/2}$ binding energies in comparison to the neutral complexes **1** and **2**; a more than 1 eV shift was observed for Cu(III) ground state complex $[\mathbf{2}]^+$. These data support that a Cu(II) valence state is maintained for $[\mathbf{1}]^+$. The X-band and Q-band EPR spectra of complex $[\mathbf{1}]^+$ showed a triplet ground state with $|D| = 0.470 \pm 0.035$ cm^{-1}, $E/D = 0.06 \pm 0.02$, and $g = 2.06$. It is noteworthy that these parameters are slightly lower than those predicted recently by CASSCF calculations for a Cu(II)-radical salen complex.[24] A possible explanation for the lower $|D|$ value in $[\mathbf{1}]^+$ may be the longer metal-phenoxyl oxygen bond distance for $[\mathbf{1}]^+$ in comparison to the previously reported 5-membered chelate salen system. On the other hand, the magnitude of $|D|$ is larger while the rhombicity is smaller than that of a square-pyramidal Cu(II)-phenoxyl complex with equatorial phenoxyl radical coordination ($|D| = 0.32$ cm^{-1} and $E/D = 0.27$ cm^{-1}).[44] This difference is ascribed to the changes in the geometry and the electronic structure between Schiff bases and Mannich bases. Further, the intensity of the bands attributed to the $S = 1$ species increased with decreasing temperature, indicating that complex $[\mathbf{1}]^+$ exhibits weak intramolecular ferromagnetic coupling between the Cu(II) and radical unpaired electron spins. From the study of the temperature dependent magnetic susceptibility, the intramolecular exchange interaction constant was estimated to be $J/k_B = 4.1$ cm^{-1} based on the $\boldsymbol{H} = -2J\boldsymbol{S}_{Cu}\cdot\boldsymbol{S}_{rad}$. The parameters for $[\mathbf{1}]^+$ suggest the orthogonality of the copper $d_{x^2-y^2}$ and phenoxyl radical π magnetic orbitals.[65] The J value is small in comparison to other Cu(II)-salen phenoxyl radical complexes, which may be due to the elongated $Cu-O_{phenoxyl}$ bond.[24] However, it is not possible at this stage to clarify the reason for the very small ferromagnetic coupling constant and large $|D|$ values, since the Cu(II)-radical complexes are rare. The results of the computational experiment support that the one-electron oxidized complex, $[\mathbf{1}]^+$, can be assigned as a Cu(II)-phenoxyl radical species. The CAM-B3LYP calculation predicts a large asymmetry in the coordination environment with localization of the phenoxyl radical on one side of the molecule.

The electronic spectrum of $[\mathbf{1}]^+$ exhibits weak and broad NIR bands, indicating the formation of a localized phenoxyl radical complex. The energies and intensities of the NIR bands for $[\mathbf{1}]^+$ are different from those of complex $[\mathbf{2}]^+$. Investigation of the low energy NIR transitions enables further analysis of the degree of electronic coupling in the oxidized complexes. Analysis of the low energy bands according to Hush demonstrates that the experimental bandwidths ($\Delta\upsilon_{1/2}$) for the oxidized complexes are significantly higher than the predicted minimum bandwidth ($\Delta\upsilon_{HTL}$) at the high temperature limit.[58−60] The two values $\Delta\upsilon_{1/2}$ and $\Delta\upsilon_{HTL}$ are estimated to be 1430 and 3910 cm^{-1}, respectively, indicating that complex $[\mathbf{1}]^+$ can be assigned as class II mixed valence complex.[55−58] TD-DFT calculations on $[\mathbf{1}]^+$ predict a βHOMO → βLUMO transition in the NIR, which is assigned as a phenolate to phenoxyl intervalence charge transfer (IVCT) transition. Thus, the phenoxyl radical complex $[\mathbf{1}]^+$ exists as a localized phenoxyl radical complex. Localization of the radical electron was also observed in the resonance Raman spectrum of $[\mathbf{1}]^+$; both the ν_{7a} and ν_{8a} phenoxyl Raman bands (1494 cm^{-1} and 1581 cm^{-1}, respectively) and the phenolate ν_{11a} band (1534 cm^{-1}) were observed. The energy and intensity of the two bands match those reported for localized Ni^{II}-phenoxyl radical complexes with the same *tert*-butyl substitution.[19] In comparison to $[\mathbf{1}]^+$, the oxidized species of the group 10 metal **Salpn** series exhibit enhanced radical delocalization across the ligand framework.[20] Because of the increased rigidity of the ligand backbone for $[\mathbf{1}]^+$ (vs 1,3-propanediamine for Salpn) the angle between the two redox-active phenolates in $[\mathbf{1}]^+$ is about 42°, limiting orbital overlap and communication between the phenolate and the phenoxyl moieties. Similar radical localization was observed for manganese salen phenoxyl radical complexes.[66]

The reactivity of complex $[\mathbf{1}]^+$ with benzyl alcohol was investigated and compared with that of the Cu(III)-phenolate ground state complex $[\mathbf{2}]^+$.[22,29] Although the reaction rate of complex $[\mathbf{1}]^+$ was about 4-times higher than that of complex $[\mathbf{2}]^+$, the overall oxidation required two molar equivalents of $[\mathbf{1}]^+$ or $[\mathbf{2}]^+$, and the rate determining step of $[\mathbf{1}]^+$ is determined to be a bimolecular reaction between benzyl alcohol and the oxidized complex. The reaction rates of $[\mathbf{1}]^+$ did not show saturation behavior, remaining linear over the substrate range up to 1.0 M, and therefore the association constant of complex $[\mathbf{1}]^+$ with benzyl alcohol could not be determined. Such a trend has been reported for the reaction kinetics of complex $[\mathbf{2}]^+$,[29] suggesting a similar reaction mechanism for $[\mathbf{1}]^+$. The detailed mechanism of the alcohol oxidation has been discussed previously; complex $[\mathbf{2}]^+$ can act as a one-electron oxidant for benzyl alcohol and oxidize it to the ketyl radical in the rate determining step. Therefore, the rate determining step involves both the substrate association with the oxidized complex and the C−H hydrogen abstraction from the benzyl alcohol. The large kinetic isotope effect (KIE = $k(H)/k(D) = 13$) of complex $[\mathbf{1}]^+$ indicates that the rate determining step involves C−H bond cleavage. The similarity in the reactivity of $[\mathbf{1}]^+$ and $[\mathbf{2}]^+$ may be understood from the activation parameters. Small differences in the parameters shown in Table 2 suggest that the activated complexes of $[\mathbf{1}]^+$ and $[\mathbf{2}]^+$ have similar reactivities for oxidation as well as similar geometries for the substrate association. The similar potentials correspond with the similar enthalpies and redox potentials for $[\mathbf{1}]^+$ and $[\mathbf{2}]^+$ ($\Delta E = 0.03$ V for the first redox wave).

The increased reaction rate for $[\mathbf{1}]^+$ in comparison to $[\mathbf{2}]^+$ can be attributed to the different electronic structure, i.e., Cu(II)-radical for $[\mathbf{1}]^+$, and Cu(III) ground state for $[\mathbf{2}]^+$ which is in equilibrium with the Cu(II)-ligand radical in solution at room temperature as reported previously.[22] The constant k_2 for the reaction of $[\mathbf{1}]^+$ corresponds to the rate constant of a simple

bimolecular process between the Cu(II)-radical and $C_6H_5CH_2OH$ (k_2*) in the rate-determining step ($k_2 = k_2$*), while in the reaction of $[\mathbf{2}]^+$, k_2 should involve an equilibrium between Cu(III) and Cu(II)-radical species (K_{pre}= [Cu(II)-radical]/[Cu(III)]) as expressed by the following equation:[63]

$$k_2 = k_2^* K_{pre}/(1 + K_{pre}) \quad (6)$$

Since complex $[\mathbf{2}]^+$ has been reported to exist in about 1:1 equilibrium between Cu(III)-phenolate and Cu(II)-phenoxyl radical species,[22] K_{pre} was estimated to be ≈1, and hence k_2 for the reaction of $[\mathbf{2}]^+$ is calculated to be $k_2 \approx k_2^*/2$. If the Cu(III) species does not react with benzyl alcohol, the k_2 value for the reaction of $[\mathbf{1}]^+$ is at least double the value for $[\mathbf{2}]^+$, assuming k_2* is the same for both systems. In addition, it is plausible that the higher reactivity of the Cu(II)-radical of $[\mathbf{1}]^+$ toward $C_6H_5CH_2OH$ may be due to the increased conformational flexibility of the 6-membered chelate ring of $[\mathbf{1}]^+$ in comparison to the 5-membered chelate 1,2-cyclohexanediamine backbone of $[\mathbf{2}]^+$.

Hydrogen abstraction acceleration may be one of the reasons for the active form of GO which contains a Cu(II)-phenoxyl radical species. However, the reaction rate of primary alcohol oxidation by GO is at least 10^4-fold faster than the two complexes reported herein and other reported Cu(II)-phenoxyl radical species.[67,68] This 10^4-fold difference in the reaction rate cannot be explained only by electronic structure differences. The present findings suggest that the small difference of geometry and flexibility because of the chelate ring size gives rise to a significant reaction rate difference. Therefore, many factors including the redox behavior of the Cu-phenolate moiety as well as the molecular environment and geometry at the active site of GO should be considered for mimicking its reactivity.

SUMMARY

We have investigated and characterized the neutral and one-electron oxidized copper(II) **1,3-Salcn** complex and compared the electronic structure and reactivity with those of the **1,2-Salcn** analogue. The six-membered chelate **1,3-Salcn** complex exhibits subtle differences in the electronic structure and oxidation reactivity with benzyl alcohol, in comparison to its 5-membered chelate analogue complex of **1,2-Salcn**. The one-electron oxidized **1,3-Salcn** complex exists as a ligand-based radical complex in solution and in the solid state, which is in contrast to the Cu(III)-phenolate ground state of the oxidized **1,2-Salcn** complex. The solid state structure of the oxidized **1,3-Salcn** complex exhibits an asymmetric coordination structure as compared with the 5-membered chelate analogue, which suggests that this complex exists as a localized phenoxyl radical in the solid state. XPS results support that the central copper ion is assigned a valence state of +II. EPR and magnetic susceptibility measurements revealed that this phenoxyl radical complex exhibits a very weak intramolecular ferromagnetic interaction between the radical and the copper unpaired electron spins. Analysis of the NIR bands for $[\mathbf{1}]^+$ indicates that this species is a Class II localized mixed valence complex. Ligand radical localization is supported by the resonance Raman measurements, which show both characteristic phenoxyl radical and phenolate Raman bands. Both $[\mathbf{1}]^+$ and $[\mathbf{2}]^+$ exhibit a similar reaction mechanism for benzyl alcohol oxidation, but the reaction rate of $[\mathbf{1}]^+$ is about 4 times faster in comparison to $[\mathbf{2}]^+$ under the same conditions. The oxidation of benzyl alcohol can be described as a second order process with the complexes without saturation kinetics, and the rate determining step for both complexes involves hydrogen abstraction. Kinetic isotope analysis suggests that the barrier for C−H bond scission is lower for $[\mathbf{1}]^+$ in comparison to $[\mathbf{2}]^+$. The activation parameters of the reaction of $[\mathbf{1}]^+$ with benzyl alcohol indicate that hydrogen abstraction is slightly more favorable in comparison to $[\mathbf{2}]^+$. The activation energy difference between $[\mathbf{1}]^+$ and $[\mathbf{2}]^+$ was estimated to be 0.6 ± 0.2 kcal mol^{-1}, which is in line with the value from the KIE measurement. This agreement indicates that the reactivity difference arises from the hydrogen abstraction mechanism, for which the localized Cu(II)-phenoxyl radical is more favorable. From these results, we suggest that the localized phenoxyl radical and possibly increased ligand flexibility accelerate benzyl alcohol oxidation. Further studies on the correlation between reactivity and electronic structure described herein are under way.

ASSOCIATED CONTENT

Supporting Information

Crystal data for complex $[\mathbf{1}]^+$ (**Table S1**), X-ray crystal structure of complex **1** (**Figure S1**), the XPS of complexes **1** and $[\mathbf{1}]^+$ (**Figure S2**), X-band EPR spectra of complex $[\mathbf{1}]^+$ (**Figure S3**), the DFT calculation data (**Table S2** and **Figure S4**), the solvent dependent NIR spectra (**Table S3** and **Figure S5**) and the kinetic data for the reactions of oxidized complexes with benzyl alcohol (**Table S4** and **Figure S6**). This material is available free of charge via the Internet at http://pubs.acs.org.

AUTHOR INFORMATION

Corresponding Author

*E-mail: yshima@mx.ibaraki.ac.jp.

Notes

The authors declare no competing financial interest.

ACKNOWLEDGMENTS

We would like to thank Prof. Tatsuo Yajima in Kansai University for XPS measurements. This work was supported by a Grant-in-Aid for Scientific Research (No. 22550055 to Y.S.) from the Ministry of Education, Culture, Sports, Science, and Technology of Japan, and by the Cooperative Research Program of Network Joint Research Center for Materials and Devices (Institute for Materials Chemistry and Engineering, Kyushu University). T.S. would like to thank NSERC for a Discovery Grant and Compute Canada and Westgrid for access to computational resources.

REFERENCES

(1) Holm, R. H.; Kennepohl, P.; Solomon, E. I. *Chem. Rev.* **1996**, *96*, 2239.

(2) Nam, W., Ed.; *Acc. Chem. Res.*, **2007**, *40*, 465−634 (Special Issue on Dioxygen Activation by Metalloenzymes and Models)

(3) (a) Sono, H.; Roach, M. P.; Coulter, E. D.; Dawson, J. H. *Chem. Rev.* **1996**, *96*, 2841. (b) Meunier, B.; de Visser, S. P.; Shaik, S. *Chem. Rev.* **2004**, *104*, 3947.

(4) (a) Baik, M.; Newcomb, M.; Friesner, R. A.; Lippard, S. J. *Chem. Rev.* **2003**, *103*, 2385. (b) Tshuva, E. Y.; Lippard, S. J. *Chem. Rev.* **2004**, *104*, 987. (c) Costas, M.; Mehn, M. P.; Jensen, M. P.; Que, L., Jr. *Chem. Rev.* **2004**, *104*, 939. (d) Solomon, E. I.; Brunold, T. C.; Davis, M. I.; Kemsley, J. N.; Lee., S.-K.; Lehnert, N.; Neese, F.; Skulan, A. J.; Yang, Y.-S.; Zhou, J. *Chem. Rev.* **2000**, *100*, 235. (e) Gunay, A.; Theopold, K. H. *Chem. Rev.* **2010**, *110*, 1060.

(5) (a) Que, L., Jr.; Tolman, W. B. *Angew. Chem., Int. Ed.* **2002**, *41*, 1114. (b) Mirica, L. M.; Ottenwaelder, X.; Stack, T. D. P. *Chem. Rev.*

2004, *104*, 1013. (c) Lewis, E. A.; Tolman, W. B. *Chem. Rev.* **2004**, *104*, 1047.
(6) Stubbe, J.; van der Donk, W. A. *Chem. Rev.* **1998**, *98*, 705.
(7) Frey, P. A.; Hegeman, A. D.; Reed, G. H. *Chem. Rev.* **2006**, *106*, 3302.
(8) (a) Whittaker, J. W. *Met. Ions. Biol. Syst.* **1994**, *30*, 315. (b) Whittaker, J. W. *Chem. Rev.* **2003**, *103*, 2347.
(9) (a) Dyrkacz, G. R.; Libby, R. D.; Hamilton, G. A. *J. Am. Chem. Soc.* **1976**, *98*, 626. (b) Hamilton, G. A.; Adolf, P. K.; de Jersey, J.; DuBois, G. C.; Dyrkacz, G. R.; Libby, R. D. *J. Am. Chem. Soc.* **1978**, *100*, 1899.
(10) Clark, K.; Penner-Hahn, J. E.; Whittaker, M. M.; Whittaker, J. W. *J. Am. Chem. Soc.* **1990**, *112*, 6433.
(11) McGlashen, M. L.; Eads, D. D.; Spiro, T. G.; Whittaker, J. W. *J. Phys. Chem.* **1995**, *99*, 4918.
(12) Jazdzewski, B. A.; Tolman, W. B. *Coord. Chem. Rev.* **2000**, *200–202*, 633.
(13) (a) Chaudhuri, P.; Wieghardt, K. *Prog. Inorg. Chem.* **2001**, *50*, 151. (b) Thomas, F. *Eur. J. Inorg. Chem.* **2007**, 2379. (c) Shimazaki, Y.; Yamauchi, O. *Indian J. Chem., Sect. A* **2011**, *50*, 383 , and references cited therein.
(14) (a) Chirik, P. J.; Wieghardt, K. *Science* **2010**, *327*, 794. (b) Holland, P. L. *Acc. Chem. Res.* **2008**, *41*, 905. (c) de Bruin, B.; Hetterscheid, D. G. H.; Koekkoek, A. J. J.; Grützmacher, H. *Prog. Inorg. Chem.* **2007**, *55*, 247.
(15) (a) Chaudhuri, P.; Verani, C. N.; Bill, E.; Bothe, E.; Weyhermüller, T.; Wieghardt, K. *J. Am. Chem. Soc.* **2001**, *123*, 2213. (b) Herebian, D.; Bothe, E.; Bill, E.; Weyhermüller, T.; Wieghardt, K. *J. Am. Chem. Soc.* **2001**, *123*, 10012.
(16) (a) Shimazaki, Y.; Tani, F.; Fukui, K.; Naruta, Y.; Yamauchi, O. *J. Am. Chem. Soc.* **2003**, *125*, 10512. (b) Shimazaki, Y.; Yajima, T.; Tani, F.; Karasawa, S.; Fukui, K.; Naruta, Y.; Yamauchi, O. *J. Am. Chem. Soc.* **2007**, *129*, 2559.
(17) (a) Rotthaus, O.; Jarjayes, O.; Thomas, F.; Philouze, C.; Del Valle, C. P.; Saint-Aman, E.; Pierre, J.-L. *Chem.—Eur. J.* **2006**, *12*, 2293. (b) Rotthaus, O.; Thomas, F.; Jarjayes, O.; Philouze, C.; Saint-Aman, E.; Pierre, J.-L. *Chem.—Eur. J.* **2006**, *12*, 6953. (c) Chiang, L.; Kochem, A.; Jarjayes, O.; Dunn, T. J.; Vezin, H.; Sakaguchi, M.; Ogura, T.; Orio., M.; Shimazaki, Y.; Thomas, F.; Storr, T. *Chem.—Eur. J.* **2012**, *18* (44), 14117–14127.
(18) Storr, T.; Wasinger, E. C.; Pratt, R. C.; Stack, T. D. P. *Angew. Chem., Int. Ed.* **2007**, *46*, 5198.
(19) Storr, T.; Verma, P.; Shimazaki, Y.; Wasinger, E. C.; Stack, T. D. P. *Chem.—Eur. J.* **2010**, *16*, 8980.
(20) Shimazaki, Y.; Arai, N.; Dunn, T. J.; Yajima, T.; Tani, F.; Ramogida, C. F.; Storr, T. *Dalton Trans.* **2011**, *40*, 2469.
(21) Shimazaki, Y.; Stack, T. D. P.; Storr, T. *Inorg. Chem.* **2009**, *48*, 8383.
(22) Storr, T.; Verma, P.; Pratt, R. C.; Wasinger, E. C.; Shimazaki, Y.; Stack, T. D. P. *J. Am. Chem. Soc.* **2008**, *130*, 15448.
(23) (a) Ray, K.; Petrenko, T.; Wieghardt, K.; Neese, F. *Dalton Trans.* **2007**, 1552. (b) Ray, K.; George, S. D.; Solomon, E. I.; Wieghardt, K.; Neese, F. *Chem.—Eur. J.* **2007**, *13*, 2783. (c) Ray, K.; Weyhermuller, T.; Neese, F.; Wieghardt, K. *Inorg. Chem.* **2005**, *44*, 5345.
(24) Orio, M.; Jarjayes, O.; Kanso, H.; Philouze, C.; Neese, F.; Thomas, F. *Angew. Chem., Int. Ed.* **2010**, *49*, 4989.
(25) Perrin, D. D.; Armarego, W. L. F.; Perrin, D. R. *Purification of Laboratory Chemicals*; Pergamon Press: Elmsford, NY, 1966.
(26) Chastain, J.; King, R. G. Jr. *Handbook of X-ray Photoelectron Spectroscopy*; Physical Electronics, Perkin-Elmer Inc: Eden Prairie, MN, 1995.
(27) Ibers, J. A.; Hamilton, W. C. *International Tables for X-Ray Crystallography*; Kynoch: Birmingham, U.K., 1974; Vol. *IV*.
(28) *Crystal Structure Analysis Package*; Rigaku Corporation: The Woodlands, TX, 1985 and 1999.
(29) (a) Pratt, R. C.; Stack, T. D. P. *J. Am. Chem. Soc.* **2003**, *125*, 8716. (b) Pratt, R. C.; Stack, T. D. P. *Inorg. Chem.* **2005**, *44*, 2367.
(30) Frisch, M. J.; Trucks, G. W.; Schlegel, H. B.; Scuseria, G. E.; Robb, M. A.; Cheeseman, J. R.; Scalmani, G.; Barone, V.; Mennucci, B.; Petersson, G. A.; Nakatsuji, H.; Caricato, M.; Li, X.; Hratchian, H. P.; Izmaylov, A. F.; Bloino, J.; Zheng, G.; Sonnenberg, J. L.; Hada, M.; Ehara, M.; Toyota, K.; Fukuda, R.; Hasegawa, J.; Ishida, M.; Nakajima, T.; Honda, Y.; Kitao, O.; Nakai, H.; Vreven, T.; Montgomery, Jr., J. A.; Peralta, J. E.; Ogliaro, F.; Bearpark, M.; Heyd, J. J.; Brothers, E.; Kudin, K. N.; Staroverov, V. N.; Kobayashi, R.; Normand, J.; Raghavachari, K.; Rendell, A.; Burant, J. C.; Iyengar, S. S.; Tomasi, J.; Cossi, M.; Rega, N.; Millam, N. J.; Klene, M.; Knox, J. E.; Cross, J. B.; Bakken, V.; Adamo, C.; Jaramillo, J.; Gomperts, R.; Stratmann, R. E.; Yazyev, O.; Austin, A. J.; Cammi, R.; Pomelli, C.; Ochterski, J. W.; Martin, R. L.; Morokuma, K.; Zakrzewski, V. G.; Voth, G. A.; Salvador, P.; Dannenberg, J. J.; Dapprich, S.; Daniels, A. D.; Farkas, Ö.; Foresman, J. B.; Ortiz, J. V.; Cioslowski, J.; Fox, D. J. *Gaussian 09*, Revision A.1; Gaussian, Inc.: Wallingford, CT, 2009.
(31) Tawada, Y.; Tsuneda, T.; Yanagisawa, S.; Yanai, T.; Hirao, K. *J. Chem. Phys.* **2004**, *120*, 8425.
(32) Yanai, T.; Tew, D. P.; Handy, N. C. *Chem. Phys. Lett.* **2004**, *393*, 51.
(33) (a) Noodleman, L. *J. Chem. Phys.* **1981**, *74*, 5737. (b) Noodleman, L.; Case, D. A. *Adv. Inorg. Chem.* **1992**, *38*, 423. (c) Noodleman, L.; Davidson, E. R. *Chem. Phys.* **1986**, *109*, 131.
(34) Shafer, A.; Horn, H.; Ahlrichs, R. *J. Chem. Phys.* **1992**, *97*, 2571.
(35) Becke, A. D. *J. Chem. Phys.* **1993**, *98*, 5648.
(36) Stephens, P. J.; Devlin, F. J.; Chabalowski, C. F.; Frisch, M. J. *J. Phys. Chem.* **1994**, *98*, 11623.
(37) (a) Gorelsky, S. I. *AOMix: Program for Molecular Orbital Analysis*; University of Ottawa: Ottawa, Canada, 2007; http://www.sg-chem.net/. (b) Gorelsky, S. I.; Solomon, E. I. *Theor. Chem. Acc.* **2008**, *129*, 57.
(38) (a) Casida, M. E. In *Recent Advances in Density Functional Methods*; Chong, D. P., Ed.; World Scientific: Singapore, 1995; p 155; (b) Stratmann, R. E.; Scuseria, G. E.; Frisch, M. J. *J. Chem. Phys.* **1998**, *109*, 8218.
(39) (a) Barone, V.; Cossi, M.; Tomasi, J. *J. Chem. Phys.* **1997**, *107*, 3210. (b) Barone, V.; Cossi, M.; Tomasi, J. *J. Comput. Chem.* **1998**, *19*, 404. (c) Miertus, S.; Scrocco, E.; Tomasi, J. *Chem. Phys.* **1981**, *55*, 117. (d) Tomasi, J.; Mennucci, B.; Cances, E. *J. Mol. Struct.* **1999**, *464*, 211.
(40) Connelly, N. G.; Geiger, W. E. *Chem. Rev.* **1996**, *96*, 877.
(41) (a) Benisvy, L.; Blake, A. J.; Collison, D.; Davies, E. S.; Garner, C. D.; McInnes, E. J. L.; McMaster, J.; Whittaker, G.; Wilson, C. *Chem. Commun.* **2001**, 1824. (b) Benisvy, L.; Blake, A. J.; Collison, D.; Davies, E. S.; Garner, C. D.; McInnes, E. J. L.; McMaster, J.; Whittaker, G.; Wilson, C. *Dalton Trans.* **2003**, 1975.
(42) Verani, C. N.; Gallert, S.; Bill, E.; Weyhermüller, T.; Wieghardt, K.; Chaudhuri, P. *Chem. Commun.* **1999**, 1747.
(43) Müller, J.; Kikuchi, A.; Bill, E.; Weyhermüller, T.; Hildebrandt, K.; Ould-Moussa, L.; Wieghardt, K. *Inorg. Chim. Acta* **2000**, *297*, 265.
(44) Bill, E.; Müller, J.; Weyhermüller, T.; Wieghardt, K. *Inorg. Chem.* **1999**, *38*, 5795.
(45) (a) Abragam, A.; Bleaney, B. *Electron Paramagnetic Resonance of Transition Ions*; Oxford University Press: London, U.K., 1970. (b) Campbell, K. A.; Yikilmaz, E.; Grant, C. V.; Gregor, W.; Miller, A.-F.; Britt, R. D. *J. Am. Chem. Soc.* **1999**, *121*, 4714.
(46) J. Krzystek, J.; Park, J.-H.; Meisel, M. W.; Hitchman, M. A.; Stratemeier, H.; Brunel, L.-C.; Telser, J. *Inorg. Chem.* **2002**, *41*, 4478.
(47) Sharrock, P.; Melnik, M. *Can. J. Chem.* **1985**, *63*, 52.
(48) (a) Kahn, O. *Molecular Magnetism*; Wiley-VCH Publishers: Weinheim, Germany, 1993. (b) Bleany, B.; Bowers, K. D. *Proc. R. Soc. London* **1952**, *A214*, 451.
(49) Yang, F.-A.; Guo, C.-W.; Chen, Y.-J.; Chen, J.-H.; Wang, S.-S.; Tung, J.-Y.; Hwang, L.-P.; Elango, S. *Inorg. Chem.* **2007**, *46*, 578.
(50) Rostov, I. V.; Amos, R. D.; Kobayashi, R.; Scalmani, G.; Frisch, M. J. *J. Phys. Chem. B* **2010**, *114*, 5547.
(51) (a) Jacquemin, D.; Michaux, C.; Perpete, E. A.; Maurel, F.; Perrier, A. *Chem. Phys. Lett.* **2010**, *488*, 193. (b) Jacquemin, D.; Perpete, E. A.; Scuseria, G. E.; Ciofini, I.; Adamo, C. *J. Chem. Theory Comput.* **2008**, *4*, 123. (c) Mikolajczyk, M. M.; Zalesny, R.; Czyznikowska, Z.; Toman, P.; Leszczynski, J.; Bartkowiak, W. *J. Mol. Model.* **2011**, *17*, 2143.

(52) Use of the CAM-B3LYP functional to explain the electronic structure in a series of symmetric one-electron oxidized Ni-salen-type complexes also results in localized electronic structures; see ref 17c.
(53) Das, T. N. *J. Phys. Chem. A* **2005**, *109*, 3344.
(54) Mukherjee, A.; McGlashen, M. L.; Spiro, T. G. *J. Phys. Chem.* **1995**, *99*, 4912.
(55) Verma, P.; Pratt, R. C.; Storr, T.; Wasinger, E. C.; Stack, T. D. P. *Proc. Natl. Acad. Sci. U. S. A.* **2011**, *108*, 18600.
(56) Robin, M. B.; Day, P. *Adv. Inorg. Chem.* **1967**, *10*, 247.
(57) Creutz, C.; Taube, H. *J. Am. Chem. Soc.* **1969**, *91*, 3988.
(58) Hush, N. S. *Prog. Inorg. Chem.* **1967**, *8*, 391.
(59) D'Alessandro, D. M.; Keene, F. R. *Chem. Soc. Rev.* **2006**, *35*, 424.
(60) Hush, N. S. *Coord. Chem. Rev.* **1985**, *64*, 135.
(61) Schnepf, R.; Sokolowski, S.; Müller, J.; Bachler, V.; Wieghardt, K.; Hildebrandt, P. *J. Am. Chem. Soc.* **1998**, *120*, 2352.
(62) Warren, J. J.; Tronic, T. A.; Mayer, J. M. *Chem. Rev.* **2010**, *110*, 6961.
(63) Espenson, J. H. *Chemical Kinetics and Reaction Mechanisms*, 2nd ed.; MacGraw-Hill: New York, 2002.
(64) (a) Wang, Y.; Stack, T. D. P. *J. Am. Chem. Soc.* **1996**, *118*, 13097. (b) Wang, Y.; DuBois, J. L.; Hedman, B.; Hodgson, K. O.; Stack, T. D. P. *Science* **1998**, *279*, 537.
(65) Müller, J.; Weyhermüller, T.; Bill, E.; Hildebrandt, P.; Ould-Moussa, L.; Glaser, T.; Wieghardt, K. *Angew. Chem., Int. Ed.* **1998**, *37*, 616.
(66) Kurahashi, T.; Fujii, H. *J. Am. Chem. Soc.* **2011**, *133*, 8307.
(67) Wacher, R. M.; Branchaud, B. P. *Biochim. Biophys. Acta* **1998**, *1384*, 43.
(68) Himo, F.; Eriksson, L. A.; Maseras, F.; Siegbahn, P. E. M. *J. Am. Chem. Soc.* **2000**, *122*, 8031.